A numerical study on the interplay between the intra-particle and interparticle characteristics in bimagnetic soft/soft and hard/soft ultrasmall nanoparticle assemblies

Franciscarlos Gomes da Silva, Marianna Vasilakaki, Rafael Cabreira Gomes, Renata Aquino, Alex Fabiano, Cortez Campos, Emmanuelle Dubois, Régine Perzynski, Jérôme Depeyrot, Kalliopi Trohidou

ARTICLE

A numerical study on the interplay between the intra-particle and interparticle characteristics in bimagnetic soft/soft and hard/soft ultrasmall nanoparticles assemblies

Received 00th January 20xx,
Accepted 00th January 20xx

DOI: 10.1039/x0xx00000x

Franciscarlos Gomes da Silva,*[a] Marianna Vasilakaki, [b] Rafael Cabreira Gomes, [a,c] Renata Aquino, [d] Alex Fabiano Cortez Campos, [d] Emmanuelle Dubois, [e] Régine Perzynski, [e] Jérôme Depeyrot [a] and Kalliopi Trohidou [b]

A mesoscopic scale approach and the Monte Carlo (MC) method has been employed to study the exchange bias behavior of ultra-small $MnFe_2O_4$ (soft)/maghemite (soft) and $CoFe_2O_4$ (hard)/maghemite (soft) nanoparticles in dense and diluted assemblies at low temperatures. The analysis of our MC results clearly shows that in the powder samples the contribution to the exchange bias field (H_{ex}) and the coercivity (H_c) comes mainly from the intraparticle core/shell structure in the hard/soft sample and that the interplay between the internal characteristics and the interparticle interactions is more important in the soft/soft samples where the dipolar strength is enhanced. In the diluted frozen ferrofluid samples where interparticle exchange interactions are absent and the role of the dipolar interactions is not significant the exchange bias effects are reducing, and they come from the intra particle structure. The variation of H_{ex} and H_c with the applied cooling field well reproduces the experimental findings and sheds light on the key mechanisms of the observed magnetic behavior. Our results demonstrate the possibility to control the magnetic behaviour of nanostructures by using properly chosen core/shell bimagnetic nanoparticles.

1. Introduction

The exchange bias (EB) effect has been discovered in 1956 on Co/CoO core/shell (CS) nanoparticles.[1–3] Later, this effect has been investigated in detail by many research groups from both theoretical[4-6] and experimental points of view.[7–11] The reason for this thorough investigation is that bimagnetic core/shell nanoparticles are becoming progressively more attractive in diverse fields such as hard magnets or magnetic recording media and biomedical applications.[12-14] In addition, thanks to the progress in controlled chemical synthesis and to the advances in technical instruments for the study of the structural-morphological and magnetic properties, it is possible to explore EB in a wide range of nanoparticle systems, such as doubly–inverted nanoparticles,[15-16] core/shell nanoparticles with different compositions,[17-18] and nano-composites.[19] In a recent review, Lopez-Ortega *et al.*[13] have given a detailed study of the magnetic behavior and applications of exchange coupled bimagnetic hard/soft and soft/hard magnetic core/shell nanoparticles. In addition, Monte Carlo studies have shed light on the role of interface and surface spins on the exchange bias properties,[4,6,20-21] in various nanoparticle systems.

The cooling field dependence of the exchange bias field and the coercivity in core/shell nanoparticles has been studied by several authors.[6,19,20-23] In these works, it has been observed that as the applied field increases the exchange bias phenomena are increasing. This is attributed to the competition between the Zeeman energy and the exchange anisotropy energy for a range of applied fields. Further increase of the applied field leads to the reduction of the exchange bias effects because the Zeeman energy starts to dominate and tends to direct the interface spins along the field.

In the assemblies of magnetic nanoparticles, interparticle interactions play important role in the exchange bias behaviour of the systems. It has been demonstrated that the interplay between internal nanoparticle characteristics and interparticle interactions determine the magnetic response of the nanoparticles to an externally applied field.[21,24-26] Indeed, in previous experimental studies, we have investigated the effect of core and shell composition to the exchange bias properties of ultra-small $MnFe_2O_4$@γ-Fe_2O_3 and $CoFe_2O_4$@γ-Fe_2O_3 core/shell nanoparticles at low temperature (a few K's).[27-30] By studying dilute and dense dispersions as well as powders, it has been demonstrated experimentally that inter and intraparticle interactions play an important role in the EB properties. Our finding showed that in concentrated frozen dispersions, the dipolar interparticle interaction reduced the exchange bias field. Interparticle exchange bias was found to dominate in powder nanoparticles samples. An open question is the role of

[a] Instituto de Física, Universidade de Brasília, Caixa Postal 04455, 70919-970, Brasília, Brazil. E-mail: franciscarlos@fis.unb.br
[b] Institute of Nanoscience and Nanotechnology, NCSR "Demokritos", Athens Greece.
[c] Departamento de Física, Universidade Federal de Santa Catarina, 88040-900, Florianópolis, Brazil.
[d] Laboratory for Environmental and Applied Nanoscience, Faculty UnB – Planaltina, University of Brasília, 73345-010, Brasília, Brazil.
[e] Sorbonne Université, Laboratoire PHENIX, 4 place Jussieu, case 51, 75005, Paris, France.

the composition and the mechanism of the observed behaviour in $MnFe_2O_4$@γ-Fe_2O_3 (soft/hard) and $CoFe_2O_4$@γ-Fe_2O_3(hard/soft) nanoparticle systems.

In the present work, we investigate systematically by Monte Carlo simulations the role of the intraparticle characteristics and their interplay with interparticle interactions in the exchange bias behaviour of the assemblies. In particular, the cooling field dependence of H_c and H_{ex} is analysed in dense and in very diluted assemblies (frozen ferrofluids) using mesoscopic scale modelling. Since in the diluted dispersions, interparticle interactions play a minor role the influence of the intraparticle characteristics is clearly revealed. In all cases we discuss the numerical results in the context of our experimental findings.[27-30]

2. The model

To model spherical $MnFe_2O_4$/γ-Fe_2O_3 nanoparticles (of diameter d ~ 3.3nm and γ-Fe_2O_3 shell thickness t_{sh} = 0.4 nm) assemblies and spherical $CoFe_2O_4$/γ-Fe_2O_3 nanoparticles (of d ~ 3.1 nm and γ-Fe_2O_3 shell thickness t_{sh} = 0.5 nm) assemblies in frozen ferrofluids (very dilute samples) and powders (dense samples), we consider systems of *N* ultra-small spherical nanoparticles with a ferrimagnetic (FiM) core/FiM shell morphology. The particles are located randomly on the nodes of a cubic lattice inside a box of dimensions 10α ×10α ×10α for the dense assembly and of dimension 20α ×20α ×20α for the diluted one, where α is the lattice spacing for the sample and it is equal to the particle diameter *D*, therefore there is no overlapping of the nanoparticles. It is important to note that the choice of this model is the appropriate one to capture the internal structure and to describe the interparticle characteristics, as discussed in reference 31.

A set of three classical spin vectors is used to describe each of the nanoparticles in the assembly: one spin for the core $\vec{S}_{ci}$ and two spins $\vec{S}_{sh1i}$ and $\vec{S}_{sh2i}$ for the two sublattices of the shell with magnetic moments $\vec{m}_{\ell,i} = m_{\ell,i}\vec{S}_{\ell,i}$ with *i*=1,…, *N* and ℓ = *c*, sh1, sh2 and $m_{\ell,i} = M_{s\_\ell,i} \times V_{\ell,i} / M_s \times V$, where M_{s_ℓ} is the saturation magnetization and V_ℓ is the volume of each nanoparticle region. M_s is the total saturation magnetization of the nanoparticle and *V* is the particle volume (Fig. 1). We have

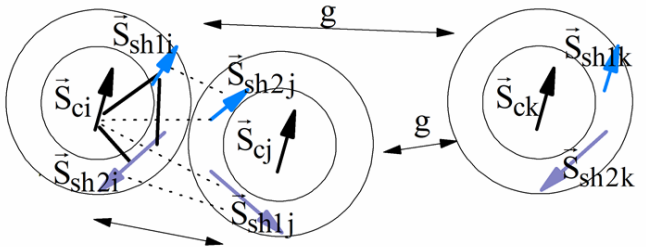

Fig 1 Schematic representation of the intra-particle and the inter-particle interactions for three random particles (i, j, k) in the assembly. Solid lines show the exchange intra-particle and the broken lines the exchange inter-particle (when the nanoparticles are in contact) interactions respectively. Double arrows show the dipolar inter-particle interactions of dipolar strength *g*.

considered one spin for the FiM core giving its net magnetic moment with uniaxial anisotropy and two for the shell because of the ultra-small size of the nanoparticle and the very small shell thickness. The two magnetic moments of the shell are randomly oriented. Therefore in the model, the core is well-ordered retaining some of the bulk characteristics and the shell is disordered, spin-glass like.[21] We introduce short range intra-particle exchange interaction between the Mn or Co ferrite core spin and each of the two maghemite shell spins (interface coupling J_{c1} and J_{c2}) and between the two shell spins (shell coupling J_{shell}). Long-range inter-particle dipolar interactions among all spins in the assemblies are considered. In the case of the dense assembly (powder sample) for the particles that are in contact, because of the very small shell thickness,[28] the particles' core spin interacts with the nearest neighbors shell spins via exchange interactions (J_{csh1}, J_{csh2}).[31] The nearest neighbours shell spins also are exchange coupled (J_{sh1sh2}).

The total energy of the system for the N nanoparticles is given by:

$$\begin{aligned}
\mathcal{E} = & -\frac{1}{2}\sum_{i=1}^{N}\left[J_{c1}\left(\vec{s}_{c,i}\cdot\vec{s}_{sh1,i}\right)+J_{c2}\left(\vec{s}_{c,i}\cdot\vec{s}_{sh2,i}\right)+J_{shell}\left(\vec{s}_{sh1,i}\cdot\vec{s}_{sh2,i}\right)\right] \\
& -K_C\sum_{i=1}^{N}\left(\vec{s}_{c,i}\cdot\hat{e}_{c,i}\right)^2-K_{sh}\sum_{i=1}^{N}\left[\left(\vec{s}_{sh1,i}\cdot\hat{e}_{sh1,i}\right)^2+\left(\vec{s}_{sh2,i}\cdot\hat{e}_{sh2,i}\right)^2\right] \\
& -\mu_0 H\sum_{i=1}^{N}\left(m_{c,i}\vec{s}_{c,i}+m_{sh1,i}\vec{s}_{sh1,i}+m_{sh2,i}\vec{s}_{sh2,i}\right)\cdot\hat{e}_h \\
& -\frac{1}{2}g\sum_{\substack{i,j=1\\ i\neq j}}^{N}\left(m_{c,i}\vec{s}_{c,i}+m_{sh1,i}\vec{s}_{sh1,i}+m_{sh2,i}\vec{s}_{sh2,i}\right)D_{ij}\left(m_{c,j}\vec{s}_{c,j}+m_{sh1,j}\vec{s}_{sh1,j}+m_{sh2,j}\vec{s}_{sh2,j}\right) \\
& -\frac{1}{2}\sum_{<i,j>}^{N}\left[J_{sh1sh2}\left(\vec{s}_{sh1,i}\cdot\vec{s}_{sh2,j}\right)+J_{csh1}\left(\vec{s}_{c,i}\cdot\vec{s}_{sh1,j}\right)+J_{csh2}\left(\vec{s}_{c,i}\cdot\vec{s}_{sh2,j}\right)\right] \qquad (1)
\end{aligned}$$

In equation 1, the first three energy terms inside the brackets describe the intra-particle Heisenberg exchange interaction between the spins in each nanoparticle, the core (c) with shell spin1(*sh1*), the core with shell spin2(*sh2*) and between the shell spins respectively. The fourth and the fifth terms give the anisotropy energy of the core and the shell spins ($\hat{e}_i$ being the random anisotropy easy-axis direction), respectively. The sixth term is the Zeeman energy ($\hat{e}_h$ being the direction of the magnetic field). The next term gives the dipolar interactions among all the spins in the assembly, where D_{ij} is the dipolar interaction tensor which in our case takes the values of the Ewald matrix.[31]

The last three terms, exist only in the case of the powder sample and describe the inter-particle exchange interactions between the neighboring shells and between the core of each nanoparticle with the neighboring shell spins respectively. There is no exchange interparticle term in the frozen ferrofluid sample.

The dipolar strength is $g = \mu_0 (M_S V)^2/4\pi d^3$, *d* being the diameter of the particle. The anisotropy constant of the core is K_C and of the shell K_{sh}, the external magnetic field is $\mu_0 H$ and the thermal energy is $k_B T$ (where *T* is the temperature). The particle volume concentration φ is taken 27% for the powder samples and 0.4% for the frozen ferrofluids.

The magnetic moments of the core and of the shell are extracted from an atomic scale model of spinel ferrite structure that takes into account explicitly the size of the shell and the core of the $MnFe_2O_4$/γ-Fe_2O_3 and $CoFe_2O_4$/γ-Fe_2O_3 nanoparticles and calculates their volumes and their saturation magnetization.

In the $MnFe_2O_4$/γ-Fe_2O_3 nanoparticles (of size d ~ 3.3nm) assemblies, the energy parameters are normalized by the volume anisotropy of the shell $K_{sh}\times V_{sh}$ so they are dimensionless. The normalized magnetic moments are: $m_c = 0.15$ for the core and $m_{sh1} = 0.50$ and $m_{sh2} = 0.58$ for the shell. In this atomic scale model the saturation magnetization has been taken 1.5 times higher from the core magnetization in agreement with the experimental results of reference 32 (M_{score} = 210 kA m^{-1} and M_s = 320 kA m^{-1}). We consider the bulk value of the $MnFe_2O_4$ for the core anisotropy ($K_c = 3\times10^3$ J m^{-3})[33] and the shell anisotropy ~ 10 times higher than the bulk maghemite anisotropy ($K_c = 5\times10^3$ J m^{-3}).[33] The reduced parameters entering our simulations for the anisotropy strength are for the core $k_C = 0.04$ and for the shell $k_{sh} = 1.0$. Our atomic scale simulations show that in the core the B sublattice is the dominant one, therefore we set the core macrospin as a "B" spin. For the intraparticle exchange coupling constant strengths between the core spin and the shell spins of the two sublattices A and B we use their bulk values for the $MnFe_2O_4$ (J_{AB} = - 22.7 K and J_{BB} = 11.5 K, $s_A = s_B = 5/2$)[34] spinel structure and the exchange coupling constants of the maghemite (J_{AB} = -25.9 K and J_{BB} = 12.7 K $s_A = s_B = 5/2$) spinel structures[34]. From the atomic scale modeling the exchange coupling constant between the A and B shell spins is found 1.44 times larger than the corresponding core value and by rescaling them we find j_{c1} = -1.6, j_{c2} = 0.8, j_{shell} = -2.3. There is not exact microscopic model for the calculation of the exchange coupling constant strengths between the nanoparticles, thus we consider for the inter-particle exchange interactions between the shell spins of particles in contact the J_{AB} of the bulk maghemite)[34] and in our model the rescaled value is j_{sh1sh2} = -0.5. The values of the core spins with the neighboring shell spins are j_{csh1} = 0.15 and j_{csh2} =-0.18. From the experimental values of M_s = 320 kA m^{-1} for the dilute sample with φ = 0.4%,[32] the dipolar strength is found to be g = 0.16. In the powder sample the experimental hysteresis loop gives enhanced saturation magnetization by a factor of 1.095 from the frozen ferrofluid samples.[35] This increase of the magnetization in the dense sample is attributed to the inter-particle exchange interactions between the particles in contact. Therefore, for the powder samples we find $g = 0.16 \times 1.2 = 0.19$.

The energy parameters of the $CoFe_2O_4$/γ-Fe_2O_3 nanoparticles (of d ~ 3.1nm) are also normalized by the factor $K_{sh}\times V_{sh}$ used in the previous system, so that we can compare the two types of samples. In this case, from our experimental findings we have that the $CoFe_2O_4$ core magnetization is lower (~ 5%) from that of the $MnFe_2O_4$ core thus the normalized magnetic moment of this core is taken m_c = 0.14. We take m_{sh1} = 0.15 and m_{sh2} = 0.8 for the maghemite shell since its volume size (t_{sh} = 0.5 nm) and the pinning parameter (p=0.03) is larger than that of the shell of the $MnFe_2O_4$/γ-Fe_2O_3 nanoparticles (t_{sh} = 0.4 nm and p = 0.01) in agreement with experiments.[28] The bulk exchange coupling constant strengths of the $CoFe_2O_4$ are :J_{AB} = -25 K and J_{BB} = 18 K, s_A = 5/2, s_B =2,[34] and using these values in our atomic scale model we find j_{c1} = -1.76, j_{c2} = 1.25, j_{shell} = -2.87. The interparticle exchange coupling strengths between the core spins with the neighboring shell spins in the $CoFe_2O_4$/γ-Fe_2O_3 nanoparticles systems are j_{csh1} = 0.165 and $j_{csh\ 2}$ = -0.28. The value of the exchange coupling constant between the shell spins of nanoparticles in contact as above is taken from the J_{AB} bulk value of maghemite[34] and in our model becomes j_{sh1sh2} = -0.62. These interparticle exchange constant values are lower than the intra-particle ones (~ 10, 4, 5 times respectively as in the system of $MnFe_2O_4$/γ-Fe_2O_3 nanoparticles).

In reference 28, it has been demonstrated that the anisotropy field of the $CoFe_2O_4$/γ-Fe_2O_3 assembly is 3 times larger than the anisotropy field of $MnFe_2O_4$/γ-Fe_2O_3 as it was estimated from the virgin magnetization curves of both systems. Therefore, if we consider that the core anisotropy has the bulk value $K_c = 2\times10^5$ J m^{-3} for $CoFe_2O_4$,[33] the increase of the effective anisotropy of the system comes from the shell. Therefore, the shell anisotropy is three times larger than that of $MnFe_2O_4$/γ Fe_2O_4 system. So, the anisotropy strengths are k_C = 1.6 for the core and k_{sh} = 3.0 for the shell. The dipolar strength for the frozen ferrofluid sample is found to be g = 0.034, much smaller than that of the $MnFe_2O_4$/γ-Fe_2O_3 assemblies, due to the smaller M_s = 160 kA m^{-1} as estimated from the experimental hysteresis loop.[28] In the powder samples, assuming the same enhancement of the saturation magnetization as in $MnFe_2O_4$/γ-Fe_2O_3 nanoparticles assemblies, we find larger g = 0.041 by a factor of 1.2.

There is experimental evidence that all the nanoparticle assemblies are polydisperse following a log-normal distribution Therefore, by introducing in our model the same particle volume polydispersity, we recalculate the corresponding volume dependent parameters, namely the magnetizations m_c,m_{sh1},m_{sh2} and the anisotropies k_C, k_{sh} for each nanoparticle of the polydisperse assembly.

3. Results and discussion

Fig. 2 gives the experimental results on the cooling field dependence of the exchange bias field H_{ex} (Fig. 2 (a,b)) together with the data of the Monte Carlo simulations (Fig. 2 (c,d)) for frozen ferrofluid (0.4%) (open symbols) and powders (closed symbols) for the $MnFe_2O_4$@ γ -Fe_2O_3 (Fig. 2 (a,c)) and $CoFe_2O_4$@γ-Fe_2O_3 (Fig. 2 (b,d)) core/shell nanoparticles respectively. In all simulations, the particle size polydispersity is included.

The calculated curves (Fig. 2 (c,d)) of the cooling field dependence of H_{ex} show a maximum (peak) in both samples in agreement with the experimental findings (Fig.2 (a,b)). The peak position is located at $H_{Cool}/K_{sh}V_{sh}$ ~ 1.5 and ~ 3.5 for $MnFe_2O_4$@γ-Fe_2O_3 and $CoFe_2O_4$@γ-Fe_2O_3 core/shell nanoparticles, respectively. These values are close to the half of the anisotropy fields given by $H_A/K_{sh}V_{sh}$ ~ 3 and $H_A/K_{sh}V_{sh}$ ~ 5 as it is estimated from the calculated virgin curves of powder samples (see Fig. 3) in qualitative agreement with the

experimental situation.[28,35] We must note here that the deviation are due to the structural difference between the experimental situation and the model. In the case of dilute dispersions (almost isolated particles) both MC results and the experimental measurements show that the maximum of H_{ex} is smaller than in powder. Moreover, the value of H_{ex} maximum is more than two times larger for the $CoFe_2O_4$@γ-Fe_2O_3 sample than for the $MnFe_2O_4$@γ-Fe_2O_3 one. This result has been attributed to a stronger pinning of the more anisotropic cores in reference 28 and indicates that the shell spin pinning through the core/ shell interface depends on the hardness of the core ferrite. [28]

Monte Carlo simulation findings indeed give larger H_{ex} values for $CoFe_2O_4$@γ-Fe_2O_3 core/shell nanoparticles in good agreement with the experimental results. For both types of samples, the measured values of H_{ex} are found larger in powders than in the diluted frozen dispersions for all the investigated range of cooling fields. This has been attributed to a collective interparticle exchange interaction acting through the multi-connected shells, which are in contact in powder samples, and are behaving as a Spin Glass-like matrix where the FI cores are embedded.[35-36] As it can be seen in Fig. 2 (c,d) Monte Carlo simulations data well reproduce this feature. This will be further enlightened in the discussion below where we study separately the contribution from the dipolar and exchange interparticle interactions. The simulation results also confirm that the interface interaction between the Co ferrite core and the spin-glass like maghemite shell, which is the origin of the H_{ex}, is rather insensitive to interparticle interactions. For $CoFe_2O_4$@γ-Fe_2O_3 nanoparticles, the ratio of the maximum H_{ex} values in both the powder and the diluted frozen liquid samples is

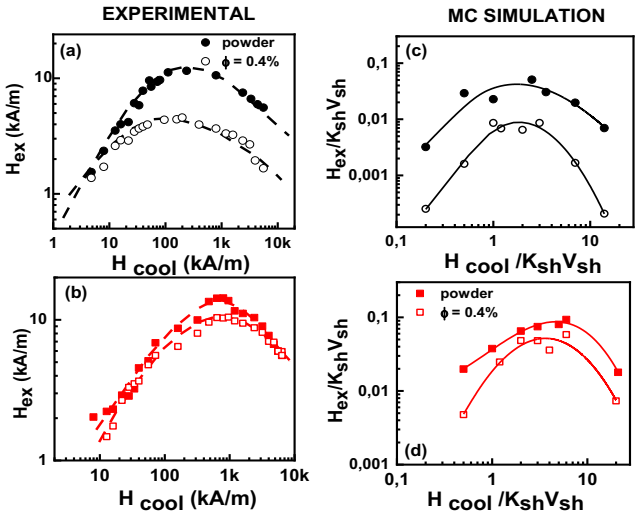

Fig 2 Cooling field dependence of the exchange bias field H_{ex} extracted from hysteresis loops. Experimental data on the left panel (a,b) are compared with Monte Carlo simulations results on the right panel (c,d) for frozen ferrofluid (open symbols) and a powder (full symbols) for the $MnFe_2O_4$@γ-Fe_2O_3 (a,c) and $CoFe_2O_4$@γ-Fe_2O_3 (b,d) core/shell nanoparticles respectively. The dashed and solid lines are guides to the eye.

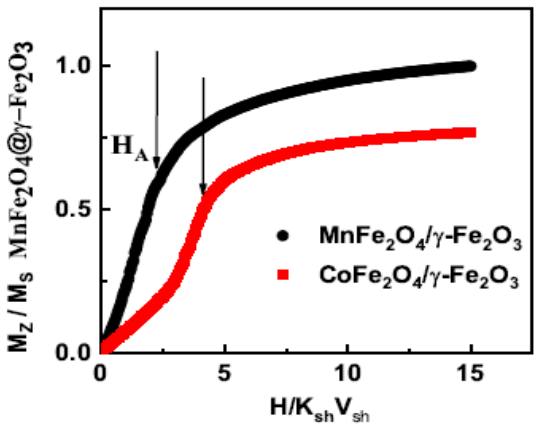

Fig 3 Calculated virgin magnetization curves for powder samples for $CoFe_2O_4$@γ-Fe_2O_3 and $MnFe_2O_4$@γ-Fe_2O_3 core/shell nanoparticles. The arrows indicate the position of the anisotropy field in both samples.

indeed 1.3 (close to the experimental ratio 1.4) and is smaller than the corresponding value found for $MnFe_2O_4$@ γ -Fe_2O_3 core/shell nanoparticles in agreement with the experimental findings.

Fig. 4 illustrates the cooling field dependence of the coercivity H_c as deduced from the hysteresis loops after field cooling. Experimental data (Fig.4 (a,b)) are compared with those obtained from Monte Carlo simulations (Fig.4 (c,d)) for frozen ferrofluid (0.4%) (open symbols) and powder (closed symbols) of $MnFe_2O_4$@γ-Fe_2O_3 (upper panel) and $CoFe_2O_4$@γ-Fe_2O_3 (lower panel) core/shell nanoparticles.

The observed behavior is completely different in the two types of core/ shell nanoparticles samples. The coercivity of

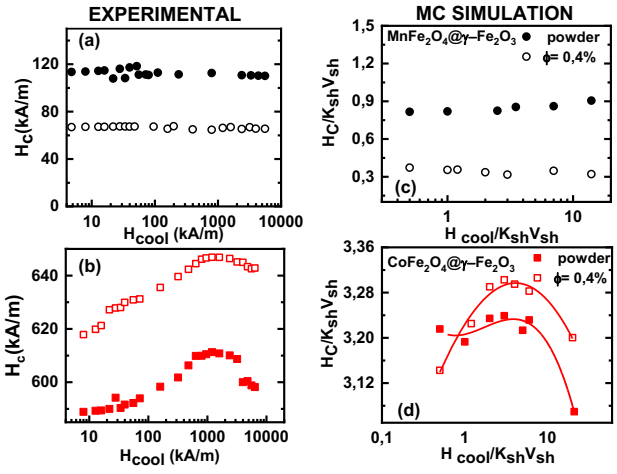

Fig 4 Cooling field dependence of the coercivity H_c Experimental data (a,b) are compared with Monte Carlo simulations results (c,d) for frozen ferrofluid (open symbols) and powder (full symbols) of the $MnFe_2O_4$@γ-Fe_2O_3 (a, c) and $CoFe_2O_4$@γ-Fe_2O_3 (b,d) core/shell nanoparticles respectively. The solid lines are guides to the eye.

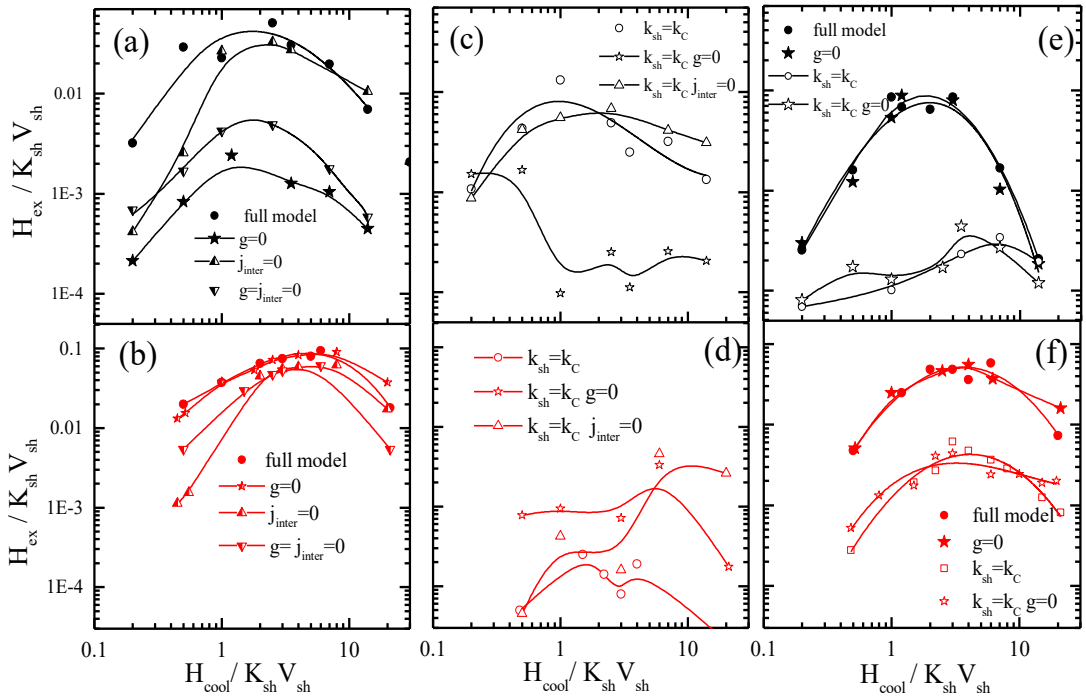

Fig 5 Monte Carlo results of the cooling field dependence of the exchange bias field H_{ex} for different values of the simulations parameters for the simulated powder samples (a,b,c,d) and the diluted frozen ferrofluids (e,f) of the $MnFe_2O_4$@γ-Fe_2O_3 (upper panel) and the $CoFe_2O_4$@γ-Fe_2O_3 (lower panel) CS nanoparticles . The solid lines are guides to the eye.

$MnFe_2O_4$@γ-Fe_2O_3core shell nanoparticles does not vary with the cooling field, whereas the curves obtained for $CoFe_2O_4$@γ-Fe_2O_3 core/shell nanoparticles exhibit a peak. These experimental findings (Fig. 4 (a,b)) are well reproduced by Monte Carlo simulations (Fig. 4 (c,d)). Also, in agreement with the experimental results, for $MnFe_2O_4$@γ-Fe_2O_3 core shell nanoparticles, the calculations show that the coercivity of the frozen liquid samples is more than 2 times smaller than in the powder ones. On the other hand, the shape of the H_c vs cooling field curves for $CoFe_2O_4$@γ-Fe_2O_3 nanoparticles is similar in the frozen dispersion and powder samples. Both in experiments and simulations, the coercivity H_c is larger in the frozen ferrofluids than in the powder samples.

In order to further investigate the contribution of the interparticle interactions, the intraparticle characteristics and their interplay in the observed magnetic behavior, MC simulations are performed for very diluted frozen ferrofluids (almost non-interacting j_{inter} = j_{sh1sh2} = j_{csh1} = j_{csh2} = 0.0), where we: a) switch off the dipolar interactions (g = 0) or b) the shell anisotropy is taken equal to the core one (setting k_{sh} = k_c) or c) we set both (k_{sh} = k_c and g = 0). In addition, in dense nanoparticles assemblies (powder samples) we switch off also either c) the exchange interparticle interaction (j_{inter} = 0) or d) all the interparticle interactions (g = j_{inter} = 0). Figs. 2 and 4 illustrate the behavior of the exchange bias field and the coercivity as a function of the cooling field respectively, for the powder samples (a,b,c,d) and the frozen diluted ferrofluid (e,f) for $MnFe_2O_4$@γ-Fe_2O_3 (upper panel) and the $CoFe_2O_4$@γ-Fe_2O_3 (lower panel) CS nanoparticles.

In Fig. 5(a,b) and 6(a,b), the results of H_{ex} and H_c vs cooling field for g = 0 (closed stars), j_{inter} = 0 (up triangles) and g= j_{inter} = 0 (down triangles) are compared with the full models $MnFe_2O_4$@γ-Fe_2O_3 and $CoFe_2O_4$@γ-Fe_2O_3 (full circles). In Fig. 5(c,d) and 6(c,d), the H_{ex} and H_c vs cooling field results for k_{sh} =k_c (open circles), k_{sh} =k_c and g = 0 (open stars), k_{sh} =k_c and j_{inter}= 0 (open up triangles) are presented. Finally, in Fig. 5(e,f) and Fig. 6 e,f the cases of diluted frozen ferrofluids with g = 0 (closed stars), k_{sh} =k_c (open circles) and k_{sh} = k_c and g = 0 (open stars) are compared with the full models $MnFe_2O_4$@γ-Fe_2O_3 and $CoFe_2O_4$@γ-Fe_2O_3 (full circles).

In $MnFe_2O_4$@γ-Fe_2O_3 powders (Fig 5a,c), H_{ex} depends significantly on the dipolar interactions because they have a large dipolar strength comparing to the anisotropy strength. The role of the intraparticle interface is not significant because of the low k_c (25 times smaller than k_{sh}), therefore the shell with the higher k is drugging the core spin. For the maximum of the H_{ex} curve, they are close to the field where the Zeeman energy competes with the shell anisotropy (because this gives the dominant contribution) and the anisotropy induced by the dipolar interactions. On the other hand, in the $CoFe_2O_4$@γ-Fe_2O_3 powders, Fig. 6 (b,d) suggests that the exchange bias mainly comes from the intraparticle interface (core/shell) and from the competition between neighbouring shells due to the interparticle exchange interactions. However, the dipolar interaction does not significantly influence the intensity of the

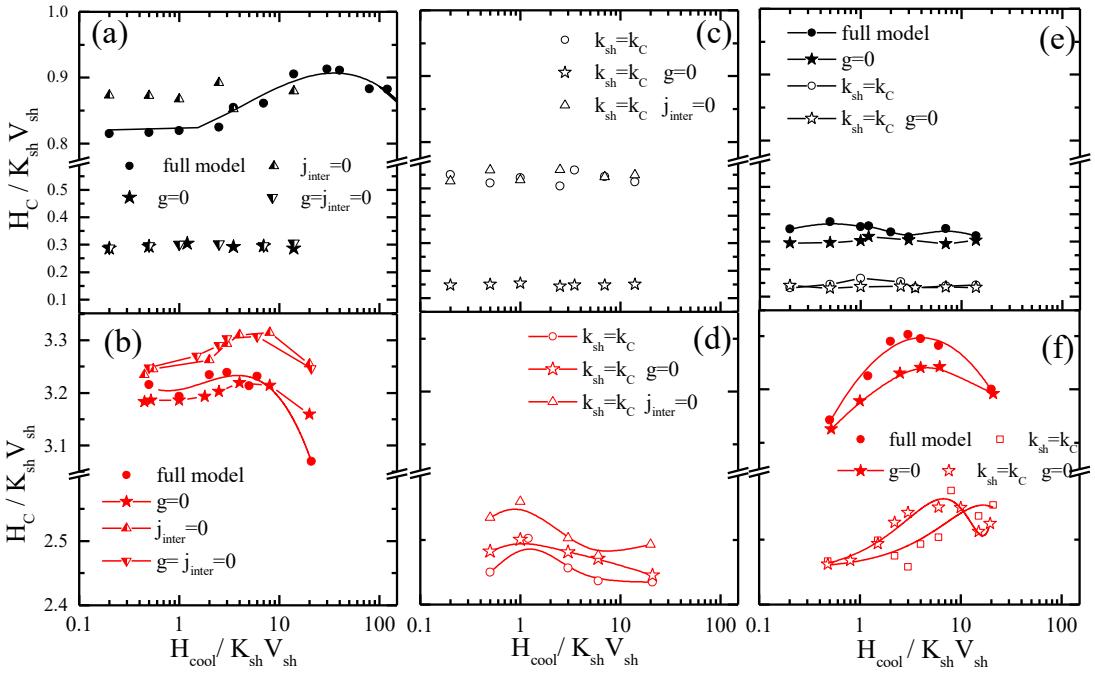

Fig 6 Monte Carlo results of the cooling field dependence of the coercivity H_c for different values of the simulations parameters, for powder samples (a,b,c,d) and diluted frozen ferrofluid (e,f) of $MnFe_2O_4$@γ-Fe_2O_3 (upper panel) and $CoFe_2O_4$@γ-Fe_2O_3 (lower panel) CS nanoparticles. The solid lines are guides to the eye.

exchange bias field fig. 5(b) (stars). The maximum H_{ex} is at the field region where the Zeeman energy competes with the shell anisotropy energy. Then when the Zeeman energy overcomes the shell anisotropy energy the spins start to align towards the field and the H_{ex} gradually reduces.

In the frozen diluted ferrofluids shown in Fig. 5 (e,f) the role of dipolar interaction is not very significant because of the low concentration. In this case, the role of j_{inter} is negligible. Moreover, if we set $k_{sh} = k_c$ in both types of nanoparticles the EB field is at least one order of magnitude lower. This does suggest that the anisotropy contrast at the interface between core and shell materials is one of the key parameters that govern exchange bias behavior. In the case of the hard core the interface competition is stronger in good agreement with experimental findings that show a larger bias for $CoFe_2O_4$@γ-Fe_2O_3 CS nanoparticles.

Fig. 6 shows the coercivity as a function of the cooling field, for the simulated powder samples (a,b,c,d) and the frozen ferrofluid (e,f) of $MnFe_2O_4$@γ-Fe_2O_3 (upper panel) and $CoFe_2O_4$@γ-Fe_2O_3 (lower panel) CS nanoparticles.

In the powder assembly of manganese ferrite/maghemite nanoparticles (Fig. 6(a,c)), the strong character of the dipolar strength that induces a strong anisotropy results to the observed large H_c and when they are switched off (g = 0 closed stars) the H_c drastically reduces, as seen in Fig. 6(a). On the other hand, the absence of interparticle exchange interactions (j_{inter} = 0 up triangles) results in a small increase of H_c. It is important to note that the absence of cooling field dependence of H_c in the cooling field range experimentally studied (in Fig. 4(a)) is due to the fact that the contribution from both shell anisotropy and dipolar interactions requires a higher cooling field to compete them. Therefore, we expect the maximum to appear at a field higher than the available for the measurements. Indeed, this is the situation in Fig. 6a (full circles) where coercivity H_c versus cooling field plot is given for a more extended cooling field range. For higher cooling field values the curve is reducing after a maximum.

In cobalt ferrite based nanoparticles samples (Fig. 6 (b,d,f)), H_c has a maximum value near the point that the Zeeman energy competes with the shell anisotropy energy. Then, it reduces for the same reason as in the H_{ex} variations (Zeeman coupling of disordered shell spins). In the case of powder assembly, the dipolar strength is small therefore it does not have significant influence on the H_c (Fig. 6(b), stars). Because of the high density of the assembly (powder), the dipolar interactions induce an ext ra anisotropy (nose to tail dipoles) and when they are switched off the coercivity H_c reduces. On the other hand, the absence of j_{inter} enhances H_c (up triangles or down triangles) because of the non-coherent rotation of the neighbouring spins. Therefore, the more significant contribution in both H_c and H_{ex} comes from the intraparticle structure and in particular from the interplay of the particle's shell anisotropy with the interparticle interactions. This can be clearly seen if we set $k_{sh} = k_c$ eliminating the shell anisotropy contribution either with (Fig. 6(d) open circles) or without interparticle interactions (Fig. 6(d) open triangles and open stars).

For the frozen diluted ferrofluid samples the influence of dipolar interactions on H_c is not significant due to the low

concentration of magnetic CS nanoparticles. Their absence results to a decrease of H_c (Fig. 6(e,f) closed stars). Finally, if the shell anisotropy is taken equal to the core one ($k_{sh} = k_c$) evidently the coercivity H_c decreases in both $MnFe_2O_4$ and $CoFe_2O_4$ based CS nanoparticles (Fig. 6 (e,f) open symbols).

4. Conclusions

We have employed our mesoscopic scale approach to simulate by MC method the exchange bias field H_{ex} and coercivity H_c in soft/soft and hard/soft ultra-small bimagnetic nanoparticles with a maghemite shell surrounding a $MnFe_2O_4$ and a $CoFe_2O_4$ core respectively. The analysis of MC results clearly shows that the more significant contribution to H_{ex} and H_c for the Co ferrite/maghemite nanoparticle comes from the intraparticle structure with the interparticle interactions to play a minor role. The interplay is stronger in manganese ferrite/maghemite nanoparticles assemblies where the dipolar interactions play a dominant role. The simulated variation of H_{ex} and H_c with the applied cooling field well reproduces the experimental findings and sheds light to the key mechanisms of the observed magnetic behavior. Our results demonstrate the possibility to control the magnetic behaviour of nanostructures by using appropriate core/shell bimagnetic nanoparticles.

Author Contributions

Franciscarlos Gomes da Silva: conceptualization, methodology, data curation, resources, writing—original draft, writing—review & editing. Marianna Vasilakaki: conceptualization, theoretical model, methodology, writing—review & editing, Rafael Cabreira Gomes: conceptualization, methodology, data curation, validation. Renata Aquino samples preparation, methodology, data curation. Alex Fabiano Cortez Campos: methodology, writing—review & editing. Emmanuelle Dubois methodology, writing—review & editing. Régine Perzynski: conceptualization, methodology, resources, writing—review & editing. Jérôme Depeyrot: conceptualization, methodology, resources, writing—original draft, writing—review & editing. Kalliopi Trohidou: conceptualization, theoretical model, methodology, writing—review & editing.

Conflicts of interest

There are no conflicts to declare.

Acknowledgements

The authors greatly acknowledge the European Union's Horizon 2020 research and innovation programme under grant agreement No. 731976 (MAGENTA). The authors of UnB and Sorbonne Université also acknowledge support by the Brazilian/French contract CAPES/COFECUB n° 88881.370915/2019-01.

References

1. W. H. Meiklejohn and C. P. Bean, *Phys. Rev.*, 1956, **102**, 1413.
2. W. Liu , W. Zhong and Y. W. Du , *J. Nanosci. Nanotechnol.*, 2008, **8**, 2781.
3. J. Nogués , J. Sort , V. Langlais , V. Skumryev , S. Suriñach , J. S. Muñoz and M. D. Baró, *Phys. Rep.*, 2005, **422**, 65.
4. E. Eftaxias and K. N. Trohidou, *Phys. Rev. B*, 2005, **71**, 134406.
5. Yong Hu, Yan Liu and An Du, *J. Magn. Magn. Mater.*, 2011 **323**, 2613–2621
6. M. Vasilakaki and K. N. N. Trohidou, *Phys. Rev. B*, 2009, **79**, 144402.
7. R. Skomski and J. M. D. Coey , *Phys. Rev. B*, 1993, **48**, 15812.
8. S. H. Moon, S. Noh, J.-H. Lee, T.-H. Shin, Y. Lim, and J. Cheon, *Nano Lett.*, 2017, **17**, 800.
9. H. Khurshid, M.-H. Phan, P. Mukherjee and H. Srikanth, *Phys. Lett.*, 2014, **104**, 072407.
10. L. Del Bianco, A. Hernando, M. Multigner, and C. Prados, *J. Appl. Phys.*, 1998, **84**, 2189.
11. G. C. Lavorato, E. Lima, Jr., H. E. Troiani, R. D. Zysler and E. L. Winkler, *Nanoscale*, 2017, **9**, 10240-10247.
12. V. Skumryev, S. Stoyanov, Y. Zhang, G. Hadjipanayis, D. Givord and J. Nogués *Nature*, 2003, **423**, 850-853.
13. A. Lopez-Ortega, M. Estarder, G. Salazar-Alvarez, A. G. Roca and J. Nogués, *Phys. Rep.*, 2015, **553**, 1–32.
14. S. Noh, S. H. Moon, T. Shin, Y. Lim and J. Cheon, *Nano Today*, 2017, **13**, 61-76.
15. I. V. Golosovsky, G. Salazar-Alvarez, A. López-Ortega, M. A. González, J. Sort, M. Estrader, S. Suriñach, M. D. Baró, and J. Nogués, *Phys. Rev. Lett.*, 2009, **102**, 247201.
16. G. Salazar-Alvarez, J. Sort, S. Surinach, M. Dolors Baro and J. Nogués, J. *Am. Chem. Soc*., 2007, **129**, 9102-9108.
17. E. Lima, Jr., E. L. Winkler, D. Tobia, H. E. Troiani, R. D. Zysler, E. Agostinelli, and D. Fiorani, *Chem. Mater.*, 2012, **24**, 512–516.
18. K. Sartori, G. Cotin, C. Bouillet, V. Halté, S. Bégin-Colin, F. Choueikani and B. P. Pichon, *Nanoscale*, 2019, **11**,12946-12958.
19. N. Flores-Martinez, G. Franceschin, T. Gaudisson, S. Haj-Khlifa, S. G. Derouich, N. Yaacoub, J. Grenèche, N. Menguy, R.l Valenzuela and S. Ammar, *Sci. Rep.*, 2019, **9**, 19468.
20. M. Vasilakaki , K. N. Trohidou and J. Nogués, *Sci. Rep.*, 2005, **5**, 9609.
21. M. Vasilakaki, G. Margaris, E. Eftaxias, and K. N. Trohidou, in *Exchange Bias From Thin Film to Nanogranular and Bulk Systems*, ed. S. K. Sharma, CRC Press, New York, 1st, 2017, vol. 1, ch. 6, pp. 127–157.
22. X. He, Y. Xu, X. Yao, C. Zhang, Y. Pu, X. Wang, W. Mao, Y. Du, and W. Zhong, *RSC Adv*., 2019, **9**, 30195.
23. L. Del Bianco, D. Fiorani, A. Testa, E. Bonetti, and L. Signorini, *Phys. Rev. B*, 2004, **70**, 52401.
24. Lavorato G C, Peddis D, Lima E, Troiani H E, Agostinelli E, Fiorani D, Zysler R D and Winkler E L 2015 *Magnetic interactions and energy barrier enhancement in core/shell bimagnetic nanoparticles* J. Phys. Chem. C 119 15755–62
25. N. Domingo, D. Fiorani, A. M. Testa, C. Binns, S. Baker and J Tejada, *J. Phys. D: Appl. Phys.*, 2008, **41**, 134009.

26. M. S. Andersson, R. Mathieu, S. S. Lee, P. S. Normile, G. Singh, P. Nordblad, and J. A. de Toro, *Nanotechnology*, 2015, **26**, 475703.
27. F. G. Silva, PhD Thesis, University of Brasília/Sorbonne Université, 2013.
28. R. Gabriera-Gomes, F. G. Silva, R. Aquino, P. Bonville, F. A. Tourinho, R. Perzynski, and J. Depeyrot, *J. Magn. Magn. Mater.*, 2014, **368**, 409.
29. R. Cabreira Gomes, F. G da Silva, T. Q. Silva, G. Gomide, V. Pilati, R. Aquino, J. Geshev, R. Perzynski, and J. Depeyrot, *J. Alloys Compd.*, 2020, **824**, 153646.
30. F. G. Silva, J. Depeyrot, Y. L. Raikher, V. I. Stepanov, I. S. Poperechny, R. Aquino, G. Ballon, J. Geshev, E. Dubois, and R. Perzynski, *Sci. Rep.*, 2021, **11**, 1.
31. G. Margaris, K. N. Trohidou, and J. Nogués, *Adv. Mater.*, 2012, **24**, 4331.
32. R, Aquino, J. Depeyrot, M. H. Souza, F. A. Tourinho, E. Dubois and R.Perzynski, *Phys. Rev.B*, 2005, **72,** 184435.
33. B. D. Cullity and C. D. Graham, *Introduction to Magnetic Materials*, John Wiley & Sons, New Jersey, 2008.
34. C. M. Srivastava, G. Srinivassan, and N. G. Nanadifar, *Phys. Rev. B*, 1979, **19**, 499.
35. F. G. Silva, R. Aquino, F. A. Tourinho, V. I. Stepanov, Y. L. Raikher, R. Perzynski, and J. Depeyrot, *J. Phys. D. Appl. Phys.*, 2013, **46**, 285003.
36. G. Margaris, M. Vasilakaki, D. Peddis, K. N. Trohidou, S. Laureti, C. Binns, E. Agostinelli, D. Rinaldi, R. Mathieu, and D. Fiorani, *Nanotechnology*, 2017, **28**, 035701.

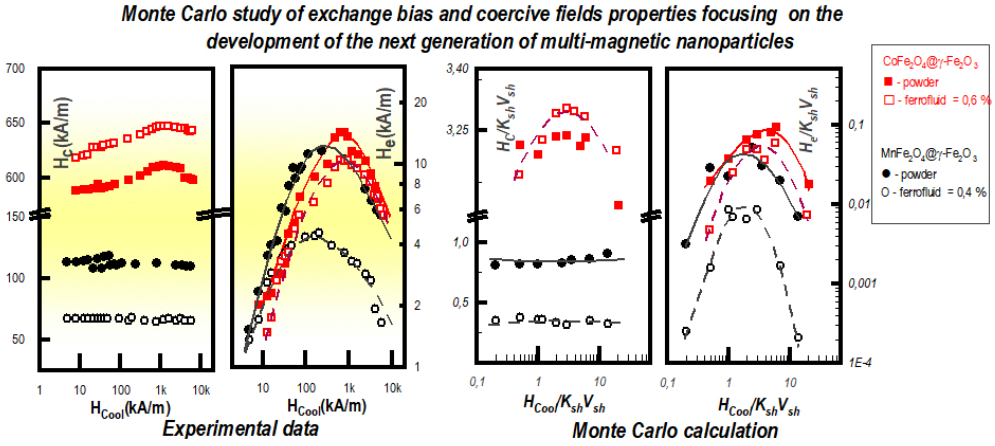

203x88mm (118 x 118 DPI)